ChemPubSoc Europe

FULL PAPERS

***Li*TR in pictures:** We identified a new class of azole-based compounds that are active against the amastigote stage of *Leishmania* parasites. Steady-state inhibition studies indicate that compound **1**, the most active, competes with trypanothione for the binding site of trypanothione reductase (TR). These results were confirmed by our determination of the X-ray crystal structure of the complex between compound **1** and TR, which shows that compound **1** impedes substrate binding to TR.

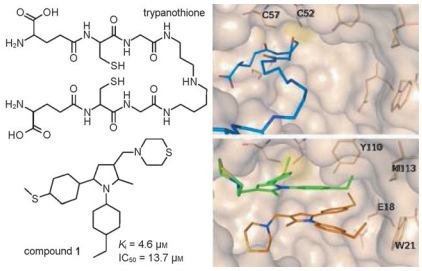

P. Baiocco, G. Poce, S. Alfonso, M. Cocozza, G. C. Porretta, G. Colotti, M. Biava,* F. Moraca, M. Botta, V. Yardley, A. Fiorillo, A. Lantella, F. Malatesta, A. Ilari*

■■ – ■■

Inhibition of *Leishmania infantum* Trypanothione Reductase by Azole-Based Compounds: a Comparative Analysis with Its Physiological Substrate by X-ray Crystallography

DOI: 10.1002/cmdc.201300176

Inhibition of *Leishmania infantum* Trypanothione Reductase by Azole-Based Compounds: a Comparative Analysis with Its Physiological Substrate by X-ray Crystallography

Paola Baiocco,[a] Giovanna Poce,[b] Salvatore Alfonso,[b] Martina Cocozza,[b] Giulio Cesare Porretta,[b] Gianni Colotti,*[c] Mariangela Biava,*[b] Francesca Moraca,[d] Maurizio Botta,[d] Vanessa Yardley,[e] Annarita Fiorillo,[a] Antonella Lantella,[a] Francesco Malatesta,[a] and Andrea Ilari[c]

Herein we report a study aimed at discovering a new class of compounds that are able to inhibit *Leishmania donovani* cell growth. Evaluation of an in-house library of compounds in a whole-cell screening assay highlighted 4-((1-(4-ethylphenyl)-2-methyl-5-(4-(methylthio)phenyl)-1*H*-pyrrol-3-yl)methyl)thiomorpholine (compound **1**) as the most active. Enzymatic assays on *Leishmania infantum* trypanothione reductase (*Li*TR, belonging to the *Leishmania donovani* complex) shed light on both the interaction with, and the nature of inhibition by, compound **1**. A molecular modeling approach based on docking studies and on the estimation of the binding free energy aided our rationalization of the biological data. Moreover, X-ray crystal structure determination of *Li*TR in complex with compound **1** confirmed all our results: compound **1** binds to the $T(SH)_2$ binding site, lined by hydrophobic residues such as Trp21 and Met113, as well as residues Glu18 and Tyr110. Analysis of the structure of *Li*TR in complex with trypanothione shows that Glu18 and Tyr110 are also involved in substrate binding, according to a competitive inhibition mechanism.

Introduction

The parasitic protozoan genus *Leishmania*, belonging to the Trypanosomatidae family, is the causative agent of leishmaniasis, a severe tropical disease. Most forms of this disease are zoonotic, in that they are transmitted via a nonhuman mammalian host, but human-to-human (anthroponotic) infections are increasing globally. Leishmaniasis consists of two main clinical forms: visceral leishmaniasis (VL), which is fatal if left untreated, and cutaneous leishmaniasis (CL), which can heal spontaneously, but leaves disfiguring scars. Mucocutaneous leishmaniasis (MCL), a sequela of *L. viannia* CL infection, is one of the hard-to-treat manifestations of this disease. Leishmaniasis is endemic in 88 countries, with more than 350 million people at risk. Each year an estimated two million people develop symptomatic leishmaniasis: among these, 0.5 million VL, and 1.5 million CL. VL causes an estimated 60000 deaths annually (a rate among parasitic diseases surpassed only by malaria).[1,2]

The pharmacological treatment of leishmaniasis relies heavily on a quartet of drugs: pentavalent antimonials (Sb^V), amphotericin B (AmpB), paromomycin, and miltefosine. The use of these drugs is associated with a number of severe side effects related to their toxicity. Moreover, an ever-increasing number of Sb^V-resistant strains have been identified in Bihar (India),[3] preventing the use of the mainstay antimonial treatment in this VL-endemic area. There is a clear need to identify novel compounds that act on new molecular targets.

This study was aimed at identifying a new class of compounds active against *Leishmania donovani*. We previously evaluated a number of synthesized compounds endowed with various biological activities: 1) 1,5-diphenylpyrroles **1**–**3**,[4–6] 1) toluidine derivatives **4**–**6**,[7,8] 3) triazolyl derivatives **7**–**11**,[9] and 4) imidazolyl derivatives **12**–**16**.[7,9] Compounds **1**–**16** were evaluated in whole-cell screens to determine their in vitro ac-

[a] *Dr. P. Baiocco, Dr. A. Fiorillo, Dr. A. Lantella, Dr. F. Malatesta*
Dipartimento di Scienze Biochimiche
Sapienza Università di Roma, Piazzale A. Moro 5, 00185 Roma (Italy)

[b] *Dr. G. Poce, Dr. S. Alfonso, Dr. M. Cocozza, Dr. G. C. Porretta, Dr. M. Biava*
Istituto Pasteur Fondazione Cenci-Bolognetti
Dipartimento di Chimica e Tecnologie del Farmaco
Sapienza Università di Roma, Piazzale A. Moro 5, 00185 Roma (Italy)
E-mail: mariangela.biava@uniroma1.it

[c] *Dr. G. Colotti, Dr. A. Ilari*
Istituto Pasteur Fondazione Cenci-Bolognetti and
Istituto di Biologia e Patologia Molecolari–CNR
c/o Dipartimento di Scienze Biochimiche
Sapienza Università di Roma, Piazzale A. Moro 5, 00185 Roma (Italy)
E-mail: gianni.colotti@uniroma1.it

[d] *Dr. F. Moraca, Dr. M. Botta*
Dipartimento di Biochimica, Chimica e Farmacia
Università degli Studi di Siena, Via Aldo Moro 2, 53100 Siena (Italy)

[e] *Dr. V. Yardley*
Faculty of Infectious & Tropical Diseases
London School of Hygiene & Tropical Medicine
Keppel Street, London WC1E 7HT (UK)

Supporting information for this article is available on the WWW under http://dx.doi.org/10.1002/cmdc.201300176.

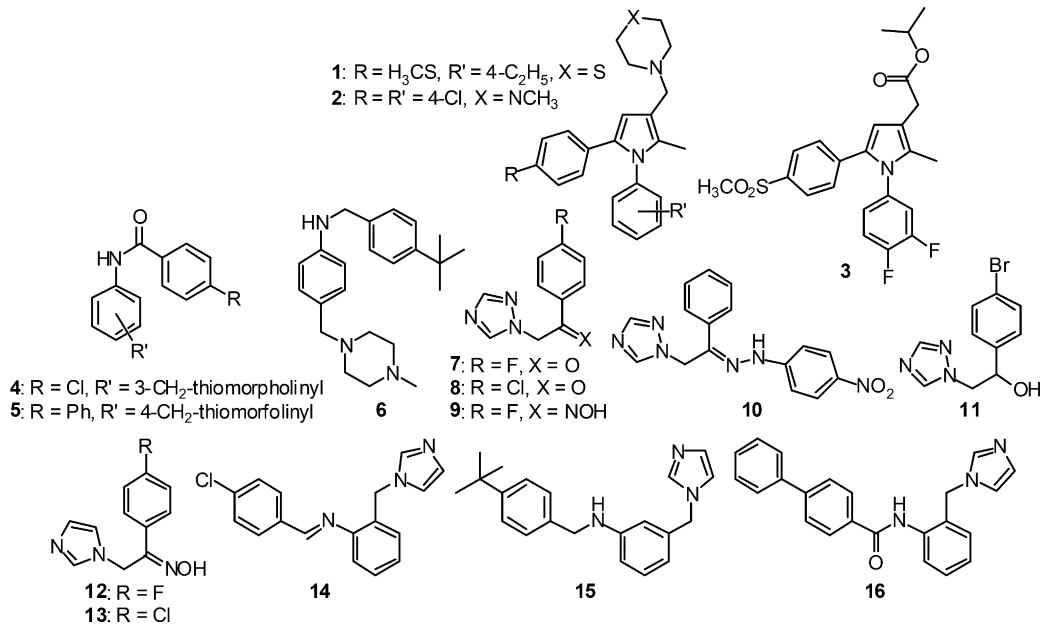

tivity against *Leishmania donovani*; among the series, compound **1** proved to be the most active.

Trypanothione reductase (TR) is unique to the parasites of the Trypanosomatidae family. It is a key component of trypanothione metabolism, which neutralizes, via the tryparedoxin/tryparedoxin peroxidase (TXN–TXNPx) couple, hydrogen peroxide produced by macrophages during infection.[10,11] TRs are members of the large and well-characterized family of FAD-dependent NAD(P)H oxidoreductases. These are dimeric flavoenzymes that catalyze the transfer of electrons between pyridine nucleotides and disulfide/dithiol compounds and promote catalysis via FAD and a redox-active disulfide (formed in TR from *Leishmania infantum* by Cys52 and Cys57), such as glutathione reductase (GR), lipoamide dehydrogenase, and mercuric ion reductase (Scheme 1).

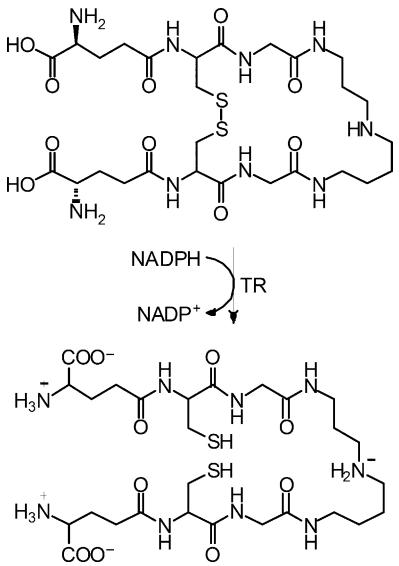

Scheme 1. Reduction of trypanothione, catalyzed by trypanothione reductase (TR).

Baiocco and colleagues[12] showed that alongside other members of the family,[13–15] *L. infantum* TR (*Li*TR) binding with NADPH induces a local conformational change in the binding domain involving residues Arg222 and Tyr198, which rotate by ~30° and 120°, respectively, around C_α–C_β to accommodate the adenine and nicotinic rings. In contrast to GR, the closest related mammalian enzyme, TR features a much wider and more hydrophobic active site which exhibits an overall negative charge.[16–19] Moreover, TR was shown to be essential for *Leishmania* parasite survival.[20] *Li*TR could be considered an attractive target for drug design, and it has been validated as a target for the development of new antileishmanial drugs by molecular genetic methods.[21,22] For these reasons we wanted to verify the inhibitory capacity of compound **1** toward *Leishmania donovani* cell growth, and to determine whether the activity is due to the inhibition of *Li*TR.

A docking study and subsequent binding free energy estimation for compounds **1**–**16** in the active site of *Li*TR were performed to rationalize the biological data, aiming at clarifying their potential binding modes. The crystallographic structure of the complex between *Li*TR and compound **1** was then determined to identify the key molecular interactions within the protein. This was compared with the X-ray crystal structure of *Li*TR in complex with the substrate, trypanothione.

Results and Discussion

Compound synthesis

Compounds **1**–**16** were prepared by following previously described synthetic pathways.[4–9]

Whole-cell screening of compounds 1–16

Activity was evaluated against the intracellular amastigote form of *Leishmania*. This is the clinically relevant stage of the

life cycle. An in vitro cytotoxicity test was performed—KB cells were exposed to the compounds for 72 h prior to evaluation—to determine if there was any selectivity. Four out of 16 compounds had IC_{50} values below the top concentration of 40 μM: in the range of 15 μM (Table 1). The activities of **1**, **2**, and **15** were similar to that of one of the positive control drugs, Sb^{V}. The IC_{50} value of **6** could not be determined; all parasites were eliminated, but the compound was toxic to host cells at the highest concentration, making accurate counts impossible. The cytotoxicity test gave a range of values. Compounds that were active in the *Leishmania* bioassay proved to be toxic to KB cells as well (Table 1).

Inhibition assay

The enzymatic activity of trypanothione reductase in the presence of compound **1** was determined by stopped-flow spectroscopy at 20 °C. The enzyme, premixed with increasing amounts of compound **1** (from 0 to 60 μM) and trypanothione at 100 μM, was mixed in the stopped-flow apparatus with a solution of 40 μM NADPH. NADPH oxidation was measured at λ 340 nm. Figure 1 shows the results of this experiment with the steady-state parameters, as obtained by nonlinear fitting, listed in Table 2. Solid lines in Figure 1 were obtained by fitting the entire data set to a closed-form solution for the total time evolution of substrate concentration (see Experimental Section below), which yields the steady-state (k_{cat} and K_M) directly. Analysis of the dependence of the steady-state parameters on compound **1** concentration (Figure 1 inset) strongly suggests a competitive inhibition mechanism with an apparent inhibition constant (K_i) of 4.6 ± 2.5 μM. The poor aqueous solubility of compound **1** contributed to the measurement uncertainty of the absorbance data, leading to a high root mean square deviation (RMSD) value.

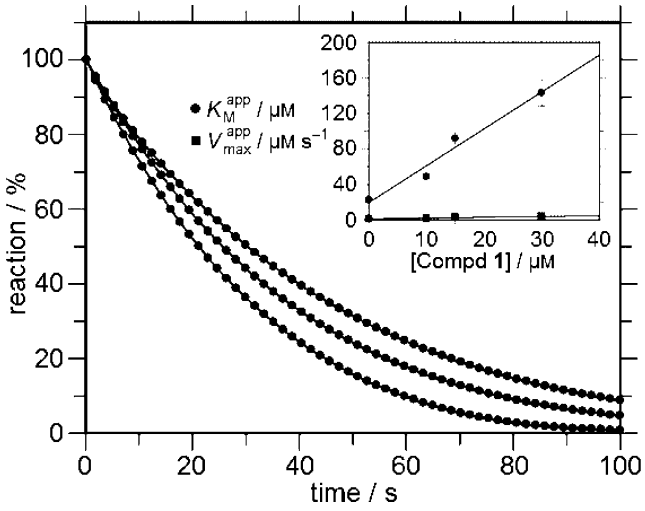

Figure 1. Time progress curves for NADPH oxidation. The enzyme (200 nM) solution in buffer, was premixed with compound **1** at 20, 30, or 60 μM (dissolved in methanol) and trypanothione at 100 μM, and kept for 15 min at $T = 298$ K. This solution was then mixed in the stopped-flow apparatus with a solution containing 33 μM NADPH. Time progress curves for NADPH oxidation were acquired at λ 340 nm and are represented as percent reaction, 100% corresponding to an absorbance of 0.103. Traces from bottom to top: 0, 10, and 30 μM compound **1** (after mixing, the 15 μM trace was removed for clarity). Solid lines were obtained by fitting the data to Equation (1) as described in the Experimental Section; 90% of the data points were removed for clarity. Inset: dependence of the steady-state parameters on compound **1** concentration.

Table 2. Steady-state parameters of TR in the presence of compound **1**.

Sample	k_{cat} [s^{-1}]	K_M [μM]	k_{cat}/K_M [$\mu M^{-1} s^{-1}$]
TR	11.4 ± 0.3	23 ± 1	0.47 ± 0.02
TR + 10 μM **1**	18.0 ± 0.4	53 ± 2	0.34 ± 0.01
TR + 30 μM **1**	19.0 ± 0.5	75 ± 2	0.25 ± 0.01

Table 1. In vitro activity of compounds **1**–**16** against *L. donovani* HU3 at various concentrations in PEM and toxicity against KB cells.

Compd	Concentration [μM]				IC_{50} [μM]	95% CI[a]	$Cytotox_{50}$
	40	13.33	4.44	1.48			
1	99.12	45.59	11.18	−0.29	13.77	12.56–15.09	12.94
2	100.00	12.06	2.35	−0.29	16.69	1.49–187.6	18.69
3	15.59	14.12	2.94	−0.59	> 40	inactive	> 100
4	−0.29	2.65	1.18	0.29	> 40	inactive	11.81
5	1.47	2.65	−1.47	−1.18	> 40	inactive	> 100
6	toxic/100[b]	29.41	4.12	−1.76	40 > *x* > 13.33	inactive	12.16
7	10.59	2.65	−0.88	−0.59	> 40	inactive	64.14
8	20.88	2.94	1.47	−0.29	> 40	inactive	15.62
9	−0.29	−0.29	−0.59	−0.59	> 40	inactive	63.38
10	19.71	22.06	4.41	−1.18	> 40	inactive	> 100
11	13.53	0.29	−0.88	0.29	> 40	inactive	> 100
12	11.76	2.35	0.59	0.29	> 40	inactive	95.73
13	15.29	14.71	9.12	9.41	> 40	inactive	83.32
14	8.53	6.47	2.94	−1.47	> 40	inactive	–
15	100.00	10.00	1.18	−2.35	16.59	0.017–16483	–
16	18.24	17.06	13.82	6.76	> 40	inactive	–
Sb^{v}	73.8	39.4	12.1	2.9	18.51	15.31–22.39	–
	1 μM	**0.33 μM**	**0.11 μM**	**0.04 μM**			
AmpB	100	99.71	86.76	50.59	0.037	0.032–0.043	

[a] Confidence interval. [b] Toxic to macrophages; no parasites present.

The inhibition constant shown by compound **1** is on the same order of magnitude as that calculated for Sb^{III} by Baiocco and co-workers ($K_i = 1.5 \pm 0.4$ μM).[12] Moreover, the K_i value of compound **1** is also on the same order of magnitude as those calculated for the competitive inhibitors of TR from other trypanosomatids. TR from *T. cruzi*, for example, was reported to be inhibited by clomipramine with an inhibition constant of 3.03 ± 0.28 μM.[23]

TR in complex with trypanothione dithiol

The crystal structure of *Li*TR in its reduced state in complex with NADPH and trypanothione was solved at 3.6 Å resolution (PDB code: 4ADW). The asymmetric unit contains a dimer of two identical subunits related by a twofold axis; superposition of the two subunits yields an RMSD of 0.31 Å. Each monomer contains a FAD and NADPH cofactor as well as a trypanothione molecule, which is located in a cleft, 15 Å wide and 20 Å deep, formed by residues from both the FAD binding site and the interface domain of the symmetry-related subunit (Figure 2). The overall structure is similar to that of the native enzyme, and the superposition with oxidized TR (PDB code: 2JK6) provides an RMSD of 0.64 Å. As previously described,[16] the catalytic site of oxidized TR is characterized by two cysteines—Cys52 and Cys57—and the His461′ residue (the prime (′) indicates residues that belong to the twofold symmetry-related subunit). In the reduced TR–$T(SH)_2$ complex, the disulfide bond between the catalytic cysteines is broken, and the residues are separated more: Cys52(Sγ)–Cys57(Sγ) = 3.2 Å. The $F_o - F_c$ difference Fourier map, contoured at 3σ, clearly shows an electron density peak in the catalytic pocket, indicating the presence of a trypanothione molecule (Figure 2A). In the catalytic site of both subunits, the γGlu-Cys-Gly motif of the trypanothione molecule adopts a U-shape and has been modeled into the $F_o - F_c$ map with an occupancy of 0.75 (Figure 2B). The sulfur (Sγ2) atom of the cysteine residue of trypanothione is hydrogen bonded to the sulfur group of Cys52 (Cys52(Sγ)–$T(SH)_2$(Sγ2) = 2.9 Å), and to the Nε2 nitrogen atom of His461′ ($T(SH)_2$(Sγ2)–His461′(Nε2) = 2.8 Å). The distance between the sulfur atom of Cys57 and the sulfur atom of trypanothione is 3.9 Å (Cys57(Sγ)–$T(SH)_2$(Sγ2); Figure 2A). Comparison of the structure of the $T(SH)_2$–*Li*TR complex with the native structure of *Li*TR (PDB code: 2JK6) in its oxidized state suggests that $T(SH)_2$ induces a movement of the loop containing the catalytic His461′ residue. In particular, the imidazole ring of His461′ is closer to Cys57 (Cys57(Sγ)–His461′(Nε2) = 2.4 Å) and moves away from Glu466′ (His461′(Nδ1)–Glu466′(Oε1) = 3.9 Å and His461′(Nδ1)–Glu466′(Oε2) = 4.1 Å). The glutathionyl tail of the trypanothione moiety is involved in hydrogen bonding with several residues of the dimerization domain and Tyr110, a residue belonging to the FAD binding domain (Figure 2B). The complete list of interactions and distances is given in Table 3. The spermidine and the second glutathionyl unit adopt an extended conformation in the trypanothione binding cavity formed at the dimeric interface. The only electrostatic interaction between trypanothione and the protein involves the glutamate residue of the second $T(SH)_2$ glutathione, which is placed at a distance of 4.3 Å from Lys240′ (Table 3, Figure 2B).

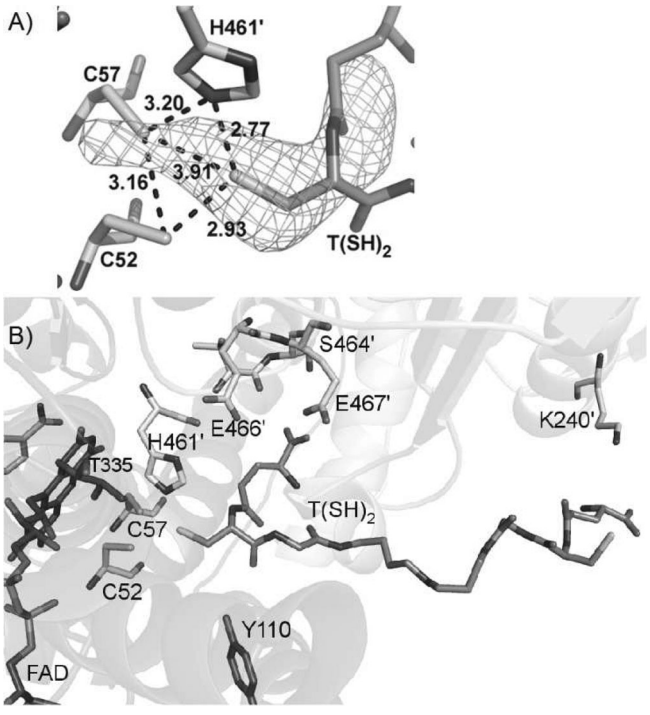

Figure 2. The trypanothione binding site. A) Spatial relationship between the cysteine residue of the first glutathionyl moiety and the two catalytic cysteines (Cys52 and Cys57). The electronic $F_o - F_c$ density map calculated without $T(SH)_2$ is indicated; the residues of the TR catalytic site and $T(SH)_2$ are depicted as sticks. B) The *Li*TR residues interacting with $T(SH)_2$ are indicated as sticks. The electrostatic interactions are shown as dotted lines. The image was generated in PyMOL.[27]

Table 3. Interactions between $T(SH)_2$ and TR.

Chain/Residue	Atom	$T(SH)_2$	*d* [Å]
Cys52	Sγ	Sγ2 (Cys1)	2.93
Cys57	Sγ	Sγ2 (Cys1)	3.91
Tyr110	OH	O2	4.18
His461′	Nε2	Sγ2 (Cys1)	2.77
His461′	Nδ1	Sγ2 (Cys1)	3.93
Glu466′	Oε2	O21 (γGlu1)	4.38
Glu467′	Oε1	O21 (γGlu1)	3.43
Thr463′	O	O11 (γGlu1)	3.05
Ser464′	Oγ	O11 (γGlu1)	4.38
Lys240′	Nζ	N7 (γGlu2)	4.32

TR in complex with compound 1

We performed a docking study of compounds **1**–**16** in the active site of the energy-minimized *Li*TR to check their orientation in the trypanothione binding site. Although the highest scores were obtained only for compounds **1**, **3**, **4**, **5**, **6**, **15**, and **16** (> 50), all the compounds were found to adopt favorable orientations inside the protein cavity, as they all show similar scoring values (Table 4). Hence, the compounds' affinities toward *Li*TR were estimated by means of the molecular mechanics/Poisson–Boltzmann surface area (MM/PBSA)

Table 4. Compounds ranked according to binding affinity against *Li*TR as estimated by the MM/PBSA method.

Compd	GoldScore	ΔG_{bind} [kcal mol^{-1}]
1	53.55	−23.50 ± 1.55
2	49.86	−21.26 ± 3.62
6	50.12	−13.24 ± 1.34
3	52.66	−12.23 ± 3.27
15	54.36	−8.78 ± 2.46
10	49.14	−6.46 ± 4.94
5	56.41	−1.41 ± 2.68
4	51.82	1.46 ± 0.62
9	39.56	4.50 ± 4.10
11	38.07	4.98 ± 5.60
12	41.92	5.13 ± 3.99
16	53.47	5.49 ± 1.47
13	43.36	7.08 ± 4.55
8	39.65	9.07 ± 4.44
7	39.13	9.11 ± 4.19
14	42.73	10.70 ± 1.62

method.[24–26] The binding free energy value predicted for compound **1** (−23.55 kcal mol^{-1}) demonstrates that it could form a more favored protein–ligand complex with respect to all the other compounds (see Experimental Section below). The crystal structure of *Li*TR in its reduced state in complex with NADPH and compound **1** (*Li*TR–**1**) was resolved at 3.2 Å (Figure 3; PDB code: 4APN). The functional dimer is composed of two identical subunits related by a twofold axis (RMSD:

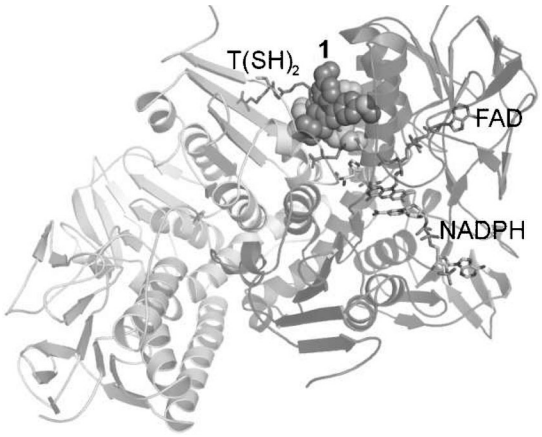

Figure 3. Overall fold of *Li*TR in complex with trypanothione and compound **1**. The FAD, NADPH, and trypanothione molecules are indicated only in one monomer and are represented as sticks. Superposition with the compound **1**–TR complex illustrates where the inhibitor binds. The two molecules of compound **1** are represented as spheres. The image was generated in PyMOL.[27]

0.18 Å). Each monomer contains a FAD unit and its NADPH cofactor, as well as two molecules of compound **1**, namely **1a** and **1b**, which are located in the trypanothione binding site (Figure 4). The overall structure is similar to that of the native enzyme and the T(SH)$_2$–*Li*TR complex, and the superpositions provide respective RMSD values of 0.37 and 0.51 Å. In the active site, the disulfide bond between the catalytic cysteines

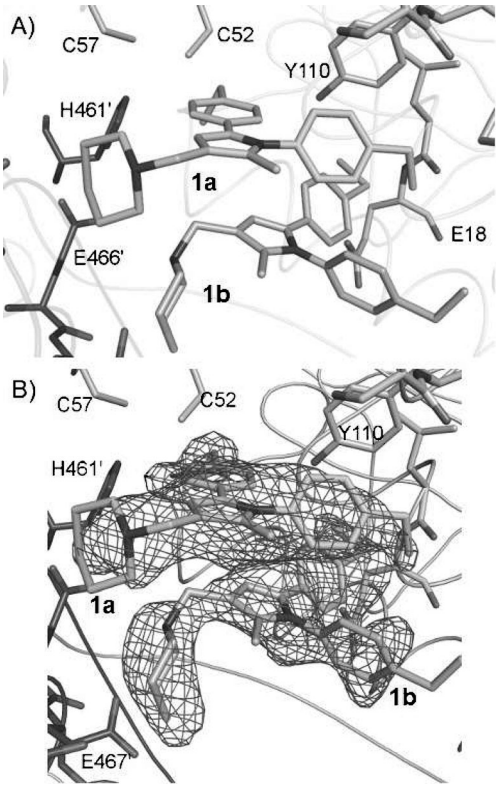

Figure 4. Close-up view of the catalytic site in the compound **1**–TR complex. A) The two inhibitors of the TR–**1** complex are depicted as sticks. The catalytic cysteines and the residues that interact with inhibitors are represented as sticks. B) $2F_o-F_c$ electronic density map of the compound **1** molecules. The image was generated in PyMOL.[27]

is broken, and the distance Cys52(Sγ)–Cys57(Sγ) is 3.4 Å. In comparison with the *Li*TR–T(SH)$_2$ complex, the catalytic His461′ is closer to Glu466′ [(His461′(Nδ1)–Glu466′(Oε1) = 3.3 Å; His461′(Nδ1)–Glu466′(Oε2) = 2.9 Å)], and the distance between His461′ and the active cysteines is greater [(His461′(Nε2)–Cys52(Sγ) = 3.2 Å; His461′(Nε2)–Cys57(Sγ) = 4.0 Å)] (Figure 4A).

Examination of the *Li*TR–**1** complex revealed that two inhibitor molecules bind in the trypanothione binding site and are involved in van der Waals interactions with residues that belong to the FAD binding domain of the monomer A and residues that belong to the interface domain of monomer B (Figure 3). In particular, superposition with the TR–T(SH)$_2$ complex shows that the inhibitor is positioned where the glutathionyl tail of trypanothione binds. Therefore, this diarylpyrrole compound inhibits TR activity by acting as a competitive inhibitor and impeding the entrance of the substrate by steric hindrance. The high flexibility of compound **1** hampered the inhibitor fitting into the F_o-F_c map, which revealed the presence of more than one conformation of both molecules in the active site. We modeled each molecule in the most populated conformation with an occupancy of 0.8, obtaining reasonable temperature factors and reasonable electron density for both compounds in the $2F_o-F_c$ map, as shown in Figure 3B. The positions of the two molecules are similar in both subunits, with the exception of the thiomorpholine ring, which is very mobile and adopts different conformations in **1a** and **1b** of the A and

B subunits. In subunit B, the ring is completely exposed to the solvent, whereas in the subunit A (Figure 4A) for both compound **1** molecules, it establishes weak interactions with some residues of the interface domain.

More importantly, the methylthiophenyl groups establish the strongest electrostatic interactions with the protein. In particular, the sulfur atom of **1a** is placed at a distance of 4.3 Å from the sulfur atom of Cys52, whereas **1b** is placed at distances of 3.8 and 4.0 Å from the N and Oε1 atoms, respectively, of Glu18 (Figure 4A). Interestingly, both molecules **1a** and **1b** may interact with the hydroxy group oxygen atom of Tyr110 (see Table 5), which is one of the residues involved in the interaction with trypanothione.

Table 5. Distances between TR residues and the two molecules of compound **1** (**1a** and **1b**; see Figure 3A).

Chain[a]/Residue	Atom	Compd **1**[b]	*d* [Å]
A/Glu18	Oε1	**b** S2	4
A/Leu17	O	**b** S2	3.4
A/Cys52	S	**a** S2	4.3
A/Ser109	Oγ	**a** N1	4.7
A/Tyr110	OH	**b** S2	4.5
A/Tyr110	OH	**a** S2	3.9
B/Glu467	Oε1	**b** S1	4.5
B/Glu467	Oε2	**b** S1	4
B/Glu467	Oε1	**b** N2	4.9
B/Ser394	Oγ	**b** S1	3.6
B/Ser395	Oγ	**a** S1	4.3
B/Thr397	O	**a** N2	4.2
B/His461	Nε2	**a** S2	5

[a] A and B are related to the two monomers of TR in the asymmetric unit. [b] S1 and N2 are the respective sulfur and nitrogen atoms that belong to the thiomorpholine ring; S2 is the sulfur atom that belongs to the methylthioaryl group.

Conclusions

The present study was aimed at identifying potentially new antileishmanial agents by elucidating the structure of TR from *Leishmania infantum* in complex with a diarylpyrrole-based compound (compound **1**), selected on the basis of whole-cell screening results. Compound **1** was found to exert a competitive inhibitory role, and the residues important for interaction with the TR protein were identified.

The crystal structure of the *Li*TR–$T(SH)_2$ complex provides structural details that explain enzyme specificity and characterizes the binding site for the disulfide substrate in terms of van der Waals interactions and hydrogen bond donors and acceptors. In addition to TRs from *T. cruzi* and *T. brucei* (*Tc*TR and *Tb*TR, respectively), previously crystallized in complex with trypanothione,[14,28] the *Li*TR structure provides the unique opportunity of having three structural pictures of the trypanothione reductase reaction. Hence, the *Tc*TR structure shows how the oxidized trypanothione binds to the enzyme. The *Tb*TR structure displays the formation of a mixed disulfide bridge as intermediate of the reaction, and finally the structure of *Li*TR, analyzed in this work, gives insight into the interaction between $T(SH)_2$ and TR after the reduction has taken place. All three structures point to a key role for Tyr110 in the formation of the complex between TR and its substrate. However, the structure of *Li*TR–$T(SH)_2$ unveils the presence of another residue, namely Lys240′, placed at the entrance of the catalytic cleft, which forms a weak electrostatic interaction with the carboxylate group of the γ-glutamate of the second glutathionyl moiety and which may play a role in driving trypanothione proximal to the two active site cysteine residues (Figure 2B).

Within a structure-based approach to drug identification, we identified a novel class of azole-based compounds that are active against the amastigote stage of *Leishmania*. The steady-state inhibition studies indicate that compound **1** competes with trypanothione for the binding site. The binding free energy estimation helped in rationalizing experimental data, showing that compound **1** binds to TR with higher affinity than the other compounds studied. These results are in agreement with the determined X-ray structure of the complex, which shows that compound **1** binds in the trypanothione binding site, thereby impeding substrate entry. Moreover, the X-ray structure of the TR–**1** complex points to the formation of a small pocket into the wide cleft where $T(SH)_2$ binds (Figure 4), in agreement with the observation of Patterson and co-workers.[28] This pocket is formed by hydrophobic residues, namely Trp21, Met113, and Glu18 or Tyr110, which interact with compound **1**, revealing a similar binding mode for different noncovalent inhibitors that bear a large hydrophobic scaffold. Moreover, these data confirm the important role of Tyr110 in the binding of both substrates and inhibitors in the TR of all members of the Trypanosomatidae family.

Experimental Section

Chemistry

^1H and ^{13}C NMR spectra were recorded with a Bruker AC400 spectrometer in the indicated solvent (TMS as internal standard); chemical shift (δ) values are expressed in ppm. Mass spectra were recorded on a API-TOF Mariner by Perspective Biosystems (Stratford, TX, USA). Compound purity was assessed by elemental analysis obtained with a PE 2400 analyzer (PerkinElmer). The purity of target compounds was $>95\%$. Analyses indicated by the elemental symbols or functions were within $\pm 0.4\%$ of theoretical values. Physicochemical and analytical data are provided in the Supporting Information.

Leishmania bioassay

Briefly, starch-induced murine peritoneal macrophages were dispensed in to Lab-Tek 16-well tissue-culture slides (Nunc, USA) and maintained at 37 °C under an atmosphere of 5% CO_2/air. After 24 h the adherent cells were infected with amastigotes harvested from the spleen of a donor mouse at a ratio of 7:1. (*L. donovani* MHOM/ET/67/HU3 in RAG1.BG mice). After a further 24 h, the level of infection was determined, and the infected cells were exposed to test drug for a total of 5 days, with the overlay + drug being changed half way through. The experiment was stopped by meth-

anol fixation and evaluated by staining the slides with 10% Giemsa for microscopic examination.[29] The percentage of infected cells was determined, each data point was taken in quadruplicate, and the percent inhibition was calculated (MS Excel) with reference to untreated controls. The IC_{50} values were calculated using Prism software.

Cytotoxicity assay

Assays were carried out as described earlier.[30] Briefly, in a 96-well plate format, KB cells (a cell line derived from a human carcinoma of the nasopharynx) were exposed to test compounds for 72 h at 37 °C under an atmosphere of 5% CO_2/air. Alamar Blue was then added to each well, followed by further incubation for 2–4 h prior to reading in a Spectra Max M3 plate reader (Molecular Devices, UK).

Inhibition assay

The enzymatic activity of trypanothione reductase was determined by stopped-flow spectroscopy at 20 °C. The aqueous solubility of compound **1** is very low: above 100 μM a manifest turbidity could be observed in the solution, and even at lower concentrations the turbidity increased with time. The experiments were therefore performed by adding the compound just before recording the data. The enzyme premixed with a methanolic solution of compound **1** (from 0 to 60 μM) and 100 μM trypanothione was mixed in the stopped-flow apparatus with a solution of 40 μM NADPH. NADPH oxidation was followed at λ 340 nm, and its concentration was determined by using an extinction coefficient at λ 340 nm of ε 6.22 $mM^{-1}cm^{-1}$. The time progress curves were fit to an explicit solution of the Michaelis–Menten time-integrated equation [Eq. (1)],[31] which was used to determine the steady-state parameters (k_{cat} and K_M) directly:

$$S = K_M \omega\left(\frac{S_0}{K_M} e^{\frac{S - k_{cat} E_0 t}{K_M}}\right) \quad (1)$$

In Equation (1) S_0 and E_0 represent the initial NADPH and total TR concentrations, respectively, and ω is the so-called Lambert W or ω function.[31] Data fitting was carried out by using Mathworks Matlab.

Molecular modeling

We minimized the energy of *Leishmania infantum* trypanothione reductase in the apo form with the ff10 force field in an orthorhombic box of TIP3P explicit solvent, with a minimum distance between any solute atom and a box edge of 8 Å using AMBER 11.[32] The minimization procedure of the protein consisted of a three-stage approach: 1) minimization of the solvent box, with harmonic restraints of 500.0 kcal mol^{-1} $Å^{-1}$ on the protein atoms; 2) minimization of the protein, with harmonic restraints of 500.0 kcal mol^{-1} $Å^{-1}$ on the solvent atoms; and 3) unrestrained minimization of the entire system. Stage 1 of the minimization consisted of 8000 steps of steepest descent followed by 2000 steps of conjugate gradient. The second stage consisted of 10000 steps of steepest descent followed by 5000 steps of conjugate gradient, while the third stage consisted of 16000 steps of steepest descent and 4000 steps using conjugate gradient. We docked compounds **1**–**16** in the active site of the minimized TR protein, using two different docking programs: Glide,[33] with both the Standard Precision (SP) and the Extra Precision (XP) methods, and GOLD 4.0[34] using all scoring functions available: ChemScore, GoldScore, ASP, and PLP. We compared the docking results obtained by means of both programs using different scoring functions within each program. We found that only with the GoldScore scoring function of GOLD was there good agreement in the docking pose of the structures with a similar scaffold, with the following parameters: 200% of efficiency, 50 runs for each ligand, and early termination turned off. We estimated the binding free energy of our compounds against the protein by means of the MM/PBSA method.[24–26]

X-ray structure determination

Cloning, expression, purification, and crystallization of TR from *Leishmania infantum* were carried out as previously reported,[12,35] and the enzyme was stored concentrated (200–400 μM) at 20 °C. Crystals of the native oxidized TR were soaked for 1 h using a stabilizing solution containing 2.5 M ammonium sulfate, 0.1 M Tris pH 8.5, and 5 mM NADPH supplemented with 2 mM trypanothione or 200 μM compound **1**. Crystals were cryoprotected in a solution containing 75% *v/v* reservoir solution and 25% *v/v* glycerol. Single-wavelength data sets (λ 0.918 Å) were collected at the beamline BL 14-1 at the Synchrotron Radiation Source BESSY[36] (Berlin, Germany) using a CCD detector at a temperature of 100 K. The data sets were processed with DENZO[36] and scaled with SCALEPACK.[37] The crystals belong to the *P*41 space group with the following cell dimensions: $a = 103.94$ Å, $b = 103.94$ Å, $c = 192.24$ Å for TR in complex with $T(SH)_2$ and $a = 102.56$ Å, $b = 102.56$ Å, $c = 191.98$ Å for TR in complex with the inhibitor. Crystal parameters and complete data collection statistics are listed in Table 6. The structures of *L. infantum* TR in complex with NADPH and trypanothione or compound **1** were solved by molecular replacement using the native TR structure (PDB code: 2JK6)[12] as search model with the program Molrep.[37] Refinement was performed using the program REFMAC5,[38] and model building was carried out with the program COOT.[39] The structure of TR in complex with $T(SH)_2$ was refined to a final R_{merge} for all resolution shells (50–3.6 Å), calculated using the working set reflections (21745) of 25%, and an R_{free} value, calculated using the test set reflections (1193) of 30%. The final model is a dimer containing 976 residues (488 for monomer A and 488 for monomer B), two FAD molecules, two NADPH molecules, and two $T(SH)_2$ molecules. The NADPH molecules were fitted into the $2F_o - F_c$ map with an occupancy of 0.75. The phenolic ring of Tyr198 was modeled with an occupancy of 0.75. The most favored regions of the Ramachandran plot contain 91.0% of residues, the allowed regions contain 9.0% of residues. The structure of TR in complex with compound **1** was refined to a final R_{merge} for all resolution shells (50–3.2 Å), calculated using the working set reflections (31061) of 23%, and an R_{free} value, calculated using the test set reflections (1660) of 27%. The final model is a dimer that contains 976 residues (488 for monomer A and 488 for monomer B), two FAD molecules, two NADPH molecules, and four molecules of compound **1**, two for each monomer in the asymmetric unit. The average of temperature factors ($B_{average}$) of the protein is 70.8 $Å^2$, while the $B_{average}$ of the inhibitors is 85 $Å^2$. The most favored regions of the Ramachandran plot contain 94.1% of residues, the allowed regions contain 5.9% of residues. All data reduction and refinement statistics are listed in Table 6. The .pdb files and dictionaries of $T(SH)_2$ and for compound **1** were generated using the PRODRG Server.[40] The atomic coordinates and structure factors have been deposited in the Protein Data Bank with PDB codes 4ADW for $T(SH)_2$-bound TR and 4APN for the TR bound with compound **1**.

Table 6. Crystal parameters, data reduction and refinement statistics.[a]

	$TR + T(SH)_2$	TR + Compd **1**
Space group	$P4_1$	$P4_1$
Unit cell [Å]	103.94, 103.94, 192.24	102.56, 102.56, 191.98
Resolution range [Å]	50–3.6 (3.7–3.6)	50–3.20 (3.3–3.2)
Total reflections (unique)	147 992 (23 097)	23 7569 (32 789)
Completeness [%]	98 (99)	100 (100)
R_{merge}	0.104 (0.372)	0.12 (0.47)
Redundancy	6.4 (6.4)	7.2 (7.3)
$\langle I/\sigma(I)\rangle$	13.8 (2.9)	16.7 (3.5)
Refinement Statistics		
Resolution range [Å]	50–3.60 (3.7–3.6)	50–3.2 (3.3–3.2)
Number of reflections	21 745 (1620)	31 061 (2280)
R_{free}	0.28 (0.38)	0.27 (0.33)
$R_{working}$	0.25 (0.34)	0.23 (0.30)
FAD	2	2
NADPH	2	2
$T(SH)_2$	2	–
Compound **15**	–	4
RMSD bond [Å]	0.01	0.01
RMSD angle [°]	1.57	1.17
Ramachandran Analysis		
Residues in most favored regions	91.7	95.8
Residues in additionally allowed regions	8.3	4.2
Outliers	0	0

[a] Values in parentheses are for the highest-resolution shell; R_{free} was calculated on 5% of data excluded before refinement.

Acknowledgements

We gratefully acknowledge the Helmholtz-Zentrum Berlin–Electron storage ring BESSY II for providing synchrotron radiation at beamline BL14-1. These studies were supported in part by the Ministero dell'Istruzione, dell'Università e della Ricerca of Italy (FIRB RBFR08F41U), the Istituto Pasteur Fondazione Cenci-Bolognetti (project: "Novel redox-sensing pathways in parasitic microorganisms"), and the European Community's Seventh Framework Programme (FP7/2007-2013) under BioStruct-X (grant agreement number 283570) and BAG-project-1223.

Keywords: leishmania · medicinal chemistry · trypanothione reductase · X-ray crystallography

[1] P. Desjeux, *Comp. Immunol. Microbiol. Infect. Dis.* **2004**, *27*, 305 – 318.
[2] P. Hotez, L. Savioli, A. Fenwick, *PLoS Neglected Trop. Dis.* **2012**, *6*, e1475.
[3] B. Y. Lee, K. M. Bacon, M. Shah, S. B. Kitchen, D. Connor, R. B. Slayton, *Am. J. Trop. Med. Hyg.* **2012**, *86*, 417 – 425.
[4] M. Biava, G. C. Porretta, G. Poce, C. Battilocchio, S. Alfonso, A. De Logu, N. Serra, F. Manetti, M. Botta, *Bioorg. Med. Chem.* **2010**, *18*, 8076 – 8084.
[5] D. Deidda, G. Lampis, R. Fioravanti, M. Biava, G. C. Porretta, S. Zanetti, R. Pompei, *Antimicrob. Agents Chemother.* **1998**, *42*, 3035 – 3037.
[6] M. Biava, G. C. Porretta, G. Poce, C. Battilocchio, F. Manetti, M. Botta, S. Forli, L. Sautebin, A. Rossi, C. Pergola, C. Ghelardini, N. Galeotti, F. Makovec, A. Giordani, P. Anzellotti, P. Patrignani, M. Anzini, *J. Med. Chem.* **2010**, *53*, 723 – 733.
[7] M. Biava, R. Fioravanti, G. C. Porretta, G. Sleiter, D. Deidda, G. Lampis, R. Pompei, *Farmaco* **1999**, *54*, 721 – 727.
[8] M. Biava, R. Fioravanti, G. C. Porretta, G. Sleiter, D. Deidda, G. Lampis, R. Pompei, A. Tafi, F. Manetti, *Med. Chem. Res.* **2002**, *11*, 50 – 66.
[9] G. C. Porretta, R. Fioravanti, M. Biava, R. Cirilli, N. Simonetti, A. Villa, U. Bello, P. Faccendini, B. Tita, *Eur. J. Med. Chem.* **1993**, *28*, 749 – 760.
[10] A. H. Fairlamb, P. Blackburn, P. Ulrich, B. T. Chait, A. Cerami, *Science* **1985**, *227*, 1485 – 1487.
[11] A. H. Fairlamb, A. Cerami, *Annu. Rev. Microbiol.* **1992**, *46*, 695 – 729.
[12] P. Baiocco, G. Colotti, S. Franceschini, A. Ilari, *J. Med. Chem.* **2009**, *52*, 2603 – 2612.
[13] Y. Zhang, C. S. Bond, S. Bailey, M. L. Cunningham, A. H. Fairlamb, W. N. Hunter, *Protein Sci.* **1996**, *5*, 52 – 61.
[14] C. S. Bond, Y. Zhang, M. Berriman, M. L. Cunningham, A. H. Fairlamb, W. N. Hunter, *Structure* **1999**, *7*, 81 – 89.
[15] S. Bailey, A. H. Fairlamb, W. N. Hunter, *Acta Crystallogr. Sect. D* **1994**, *50*, 139 – 154.
[16] C. B. Lantwin, I. Schlichting, W. Kabsch, E. F. Pai, R. L. Krauth-Siegel, *Proteins* **1994**, *18*, 161 – 173.
[17] J. Kuriyan, X. P. Kong, T. S. Krishna, R. M. Sweet, N. J. Murgolo, H. Field, A. Cerami, G. B. Henderson, *Proc. Natl. Acad. Sci. USA* **1991**, *88*, 8764 – 8768.
[18] W. N. Hunter, S. Bailey, J. Habash, S. J. Harrop, J. R. Helliwell, T. Aboagye-Kwarteng, K. Smith, A. H. Fairlamb, *J. Mol. Biol.* **1992**, *227*, 322 – 333.
[19] V. S. Stoll, S. J. Simpson, R. L. Krauth-Siegel, C. T. Walsh, E. F. Pai, *Biochemistry* **1997**, *36*, 6437 – 6447.
[20] C. Dumas, M. Ouellette, J. Tovar, M. L. Cunningham, A. H. Fairlamb, S. Tamar, M. Olivier, B. Papadopoulou, *EMBO J.* **1997**, *16*, 2590 – 2598.
[21] C. D'Silva, S. Daunes, *Expert Opin. Investig. Drugs* **2002**, *11*, 217 – 231.
[22] J. Tovar, M. L. Cunningham, A. C. Smith, S. L. Croft, A. H. Fairlamb, *Proc. Natl. Acad. Sci. USA* **1998**, *95*, 5311 – 5316.
[23] D. C. Jonesa, A. Arizaa, W. A. Chow, S. L. Oza, A. H. Fairlamb, *Mol. Biochem. Parasitol.* **2010**, *169*, 12 – 19.
[24] J. Åqvist, V. B. Luzhkov, B. O. Brandsdal, *Acc. Chem. Res.* **2002**, *35*, 358 – 365.
[25] P. A. Kollman, I. Massova, C. Reyes, B. Kuhn, S. H. Huo, L. Chong, M. Lee, T. Lee, Y. Duan, W. Wang, O. Donini, P. Cieplak, J. Srinivasan, D. A. Case, T. E. Cheatham III, *Acc. Chem. Res.* **2000**, *33*, 889 – 897.
[26] M. Mori, F. Manetti, M. Botta, *J. Chem. Inf. Model.* **2011**, *51*, 446 – 454.
[27] The PyMOL Molecular Graphics System, Version 1.1.4, Schrödinger, LLC.
[28] S. Patterson, M. S. Alphey, D. C. Jones, E. J. Shanks, I. P. Street, J. A. Frearson, P. G. Wyatt, I. H. Gilbert, A. H. Fairlamb, *J. Med. Chem.* **2011**, *54*, 6514 – 6530.
[29] V. Yardley, F. Gamarro, S. L. Croft, *Antimicrob. Agents Chemother.* **2010**, *54*, 5356 – 5358.
[30] J. O'Brien, I. Wilson, T. Orton, F. Pognan, *Eur. J. Biochem.* **2000**, *267*, 5421 – 5426.
[31] R. M. Corless, M. Gonnett, G. H. Hare, D. E. G. Jeffrey, D. E. Knuth, *Adv. Comput. Math* **1996**, *5*, 329 – 359.
[32] D. A. Case, T. A. Darden, T. E. Cheatham III, C. L. Simmerling, J. Wang, R. E. Duke, R. Luo, R. C. Walker, W. Zhang, K. M. Merz, B. Roberts, B. Wang, S. Hayik, A. Roitberg, G. Seabra, I. Kolossváry, K. F. Wong, F. Paesani, J. Vanicek, X. Wu, S. R. Brozell, T. Steinbrecher, H. Gohlke, Q. Cai, X. Ye, J. Wang, M.-J. Hsieh, G. Cui, D. R. Roe, D. H. Mathews, M. G. Seetin, C. Sagui, V. Babin, T. Luchko, S. Gusarov, A. Kovalenko, P. A. Kollman, AMBER 11, University of California, San Francisco, **2010**.
[33] Glide, Version 5.7, Schrödinger, LLC, New York, NY (USA), **2011**.
[34] M. L. Verdonk, J. C. Cole, M. J. Hartshorn, C. V. Murray, R. D. Taylor, *Proteins* **2003**, *52*, 609 – 623.

[35] P. Baiocco, S. Franceschini, A. Ilari, G. Colotti, *Protein Pept. Lett.* **2009**, *16*, 196 – 200.
[36] U. Mueller, N. Darowski, M. R. Fuchs, R. Förster, M. Hellmig, K. S. Paithankar, S. Pühringer, M. Steffien, G. Zocher, M. S. Weiss, *J. Synchrotron Radiat.* **2012**, *19*, 442 – 449.
[37] Z. Otwinowski, *Methods Enzymol.* **1997**, *276*, 307 – 326.
[38] A. Vagin, A. Teplyakov, *J. Appl. Crystallogr.* **1997**, *30*, 1022 – 1102.
[39] G. N. Murshudov, A. A. Vagin, E. J. Dodson, *Acta Crystallogr. Sect. D* **1997**, *53*, 240 – 255.
[40] P. Emsley, K. Cowtan, *Acta Crystallogr. Sect. D* **2004**, *60*, 2126 – 2132.

Received: April 19, 2013
Published online on ■■ ■■, 0000